Journal of Hazardous Materials 179 (2010) 424–430

Contents lists available at ScienceDirect

Journal of Hazardous Materials

journal homepage: www.elsevier.com/locate/jhazmat

Preparation of Al–Ce hybrid adsorbent and its application for defluoridation of drinking water

Han Liu [a], Shubo Deng [a,b,*], Zhijian Li [a,b], Gang Yu [a,b], Jun Huang [a,b]

[a] Department of Environmental Science and Engineering, Tsinghua University, Beijing 100084, China
[b] POPs Research Center, Tsinghua University, Beijing 100084, China

ARTICLE INFO

Article history:
Received 26 October 2009
Received in revised form 18 January 2010
Accepted 5 March 2010
Available online 12 March 2010

Keywords:
Fluoride
Defluoridation
Al–Ce adsorbent
Adsorption capacity
Adsorption mechanism

ABSTRACT

A novel Al–Ce hybrid adsorbent with high sorption capacity for fluoride was prepared through the coprecipitation method in this study, and its preparation conditions were optimized. X-ray diffraction (XRD) and scanning electron microscope (SEM) results showed that the hybrid adsorbent was of amorphous structure and constituted by some aggregated nanoparticles. As the adsorbent had the zero point of ζ potential at pH 9.6, it was very effective in fluoride removal from aqueous solution via electrostatic interaction. The results of sorption experiments including sorption kinetics, isotherms, and the effect of solution pH showed that the sorption of fluoride on the Al–Ce adsorbent was fast and pH-dependent. Especially, the adsorbent had high sorption capacity up to 27.5 mg g^{-1} for fluoride at the equilibrium fluoride concentration of 1 mg L^{-1}, much higher than that of the conventional adsorbents. Fourier transform infrared (FTIR) analysis and zeta potential measurement showed that the hydroxyl groups and the protonated hydroxyl groups on the adsorbent surface were involved in the fluoride adsorption.

1. Introduction

Fluoride in drinking water may be beneficial or detrimental depending on its concentration and total amount consumed. Excessive fluoride intake can affect the metabolism of elements in human body and lead to dental and bone fluorosis [1]. The acceptable fluoride concentration in drinking water is generally in the range of 0.5–1.5 mg L^{-1}. A guideline value of 1.5 mg L^{-1} was recommended by World Health Organization (WHO), but this is not a fixed value and it is intended to be adapted to take account of local conditions [2]. In China, the standard of fluoride concentration in drinking water is 1.0 mg L^{-1}. High level of fluoride in groundwater is a world-wide problem. The drinking water sources in India have been reported with fluoride concentration as high as 30 mg L^{-1} [3]. In China over 60 million people in over 20 provinces are influenced by the high fluoride concentration in drinking water, especially in some rural areas [4]. Therefore, decreasing fluoride concentration in groundwater is an important issue.

Some treatment techniques such as chemical precipitation, sorption, ion exchange, reverse osmosis, nanofiltration, and electrodialysis have been studied for defluoridation of water [5–7]. Among these methods, adsorption is one of the important techniques used for fluoride removal from water because of its ease of operation and cost-effectiveness, especially for individual homes and small community systems in rural area. Different adsorbents including activated alumina [8], bone char [9], synthetic ion exchangers [10], layered double hydroxides [11], and other natural materials have been used for fluoride removal [12]. Among them, activated alumina is the most common sorbent widely used for defluoridation of drinking water, but its optimal adsorption often works at low pH values, that increases dissolved aluminum in treated water. Since the sorption capacity of fluoride on most conventional adsorbents is not satisfactory, much effort has been devoted to develop new and cost-effective fluoride adsorbents in recent years.

It has been reported that La(III), Ce(IV), and Zr(IV) oxides had high sorption capacity for fluoride [13,14]. Since these metals are expensive, some cheaper components are commonly mixed with these metals to prepare the composite adsorbents. The hybrid adsorbents including the Fe(III)–Zr(IV) hybrid oxide [15], La(III)-modified chitosan [16], Zr(IV)-impregnated collagen fiber [17], as well as La(III) and ZrO(II) loaded zeolite [18] were reported to have high sorption capacity for fluoride. Some other bimetal adsorbents such as manganese-oxide-coated alumina [3] and Fe(III)–Al(III) mixed oxide [19] were also prepared and used to remove fluoride from aqueous solution. Wu et al. reported that the Fe–Al–Ce trimetal oxide adsorbent was very effective in fluoride removal

* Corresponding author at: Department of Environmental Science and Engineering, Tsinghua University, Beijing 100084, China. Tel.: +86 10 62792165; fax: +86 10 62794006.
E-mail address: dengshubo@tsinghua.edu.cn (S. Deng).

0304-3894/$ – see front matter © 2010 Elsevier B.V. All rights reserved.
doi:10.1016/j.jhazmat.2010.03.021

[20]. However, the Al–Ce hybrid adsorbent has not been reported to remove fluoride.

In this study, the novel Al–Ce hybrid adsorbent with high sorption capacity for fluoride was prepared through the precipitation method. The preparation conditions were optimized, and the best adsorbent was characterized by FTIR, scanning electron microscopy and energy dispersive X-ray spectroscopy (SEM-EDX), and XRD analysis. Finally, the sorption experiments including sorption kinetics, isotherm, as well as the effect of solution pH and competing anions were studied in detail, and the possible sorption mechanisms were also discussed.

2. Materials and methods

2.1. Materials

The chemicals including $Ti(SO_4)_2$, $Ce(NO_3)_3{\cdot}6H_2O$, $AlCl_3{\cdot}6H_2O$, $La_2(SO_4)_3{\cdot}9H_2O$, and $Zr(NO_3)_4{\cdot}3H_2O$ were of reagent grade and were purchased from Sinopharm Chemical Regent Co., Ltd. (China). 1000 mg L^{-1} of fluoride stock solution was prepared by dissolving NaF in 1 L of deionized water from a Milli-Q water system. The fluoride concentration was denoted as the concentration of elemental F.

2.2. Adsorbent preparation

Different metallic salts were added into 0.2 mol L^{-1} $AlCl_3$ solution at a predetermined M/Al molar ratio of 1/4. NaOH solution was added dropwise into the mixture solution until the solution pH reached 6 under vigorous stirring at 25 °C. The precipitate obtained was filtered and rinsed with deionized water, and then dried in an oven at 80 °C for 24 h. Finally, the dried product was ground into fine powder, and the adsorbent in the size range of 74–150 μm was used in this study.

2.3. ζ Potential measurement

A 10 mg aliquot of the Al–Ce adsorbent before and after fluoride sorption was placed into 100 mL of deionized water, and then the solution pH was adjusted with NaOH or HCl solution to a desired value. After 10 h stabilization, the solution pH was recorded, and the supernatant with small particles was used to conduct ζ potential measurements with a zeta potential instrument (Beckman Coulter Inc., USA). All data were determined 10 times, and the average value was adopted.

2.4. XRD analysis

X-ray powder diffraction analysis was carried out in D/max-IIIV powder diffractometer using Cu Kα radiation (λ = 1.5418 Å) at a scanning range of 2θ = 10–90° with a speed of 6° min^{-1} and a scan step of 0.02°. The adsorbent samples including the Al–Ce hybrid adsorbent prepared with different drying temperature and Ce/Al ratio, aluminum (hydr)oxide, and cerium (hydr)oxide were analyzed.

2.5. FTIR spectroscopy

The samples of the Al–Ce adsorbent before and after sorption of fluoride and co-existing ions were blended with KBr, and then pressed into a disk for FTIR analysis. Pure KBr disk was used as FTIR reference. Scans were repeated 32 times in the wavenumber range of 400–4000 cm^{-1} and the spectra were recorded on a FTIR spectrophotometer under ambient conditions.

2.6. SEM-EDX analysis

The surface morphology of the adsorbents was observed by a scanning electron microscope (JSM-6460LV). Prior to the SEM measurements, the samples were coated with Au on the surface for electric conductivity. Energy dispersive X-ray spectroscopy (JSM-6460LV) was used to measure the element composition on the adsorbent surface.

2.7. Sorption experiments

Batch sorption experiments were conducted to examine the adsorption isotherm, sorption kinetics, as well as the effect of solution pH and co-existing anions on the adsorption. In the sorption isotherm experiments, 0.01 g adsorbent was added to 100 mL fluoride solution at the concentration from 2 to 15 mg L^{-1}, and the solution pH was adjusted to 6 and controlled constant throughout the sorption experiment. The flasks were shaken at 150 rpm in a thermostatic shaker at 25 °C for 24 h. The adsorption kinetic experiments were carried out at initial fluoride concentration of 5 or 10 mg L^{-1}, and the solution pH value was 6. In the experiments for the effect of solution pH, the fluoride concentration was 10 mg L^{-1}, and the solution pH values were controlled during the sorption process. The effects of co-existing anions on the fluoride sorption were conducted in 10 mg L^{-1} fluoride solution, and the solution pH values were adjusted to 6 after the addition of Na_2CO_3, Na_2HPO_4, NaCl, Na_2SO_4, or Na_2SiO_3. After the sorption experiments, the adsorbent was separated from the solution by a filter with a 0.22 μm cellulose membrane, and the residual fluoride concentration in solution was measured by a fluoride meter equipped with fluoride ion selective electrode (Thermo Orion, USA). The sorption capacity of the adsorbent for fluoride was calculated according to the fluoride concentration difference before and after the sorption.

3. Results and discussion

3.1. Preparation optimization

3.1.1. Effect of different metals

Different metallic salts were separately added to $AlCl_3$ solution to coprecipitate the mixture, and the sorption capacity of the hybrid adsorbents for fluoride is shown in Fig. 1. It can be seen that the hybrid adsorbents containing Ce, La or Zr had higher sorption capacity than that of the Al adsorbent, while the Al–Ti hybrid adsorbent had the lowest sorption capacity for fluoride. This result

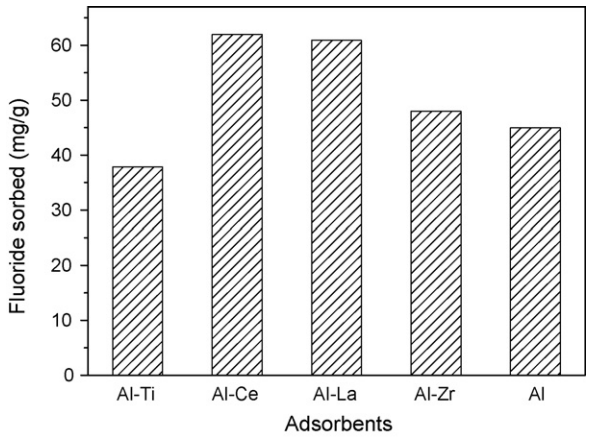

Fig. 1. Sorption of fluoride on the different hybrid adsorbents prepared by the precipitation method (sorption conditions: 0.01 g adsorbent in 100 mL of 10 mg L^{-1} fluoride solution at pH 6 and 25 °C for 24 h).

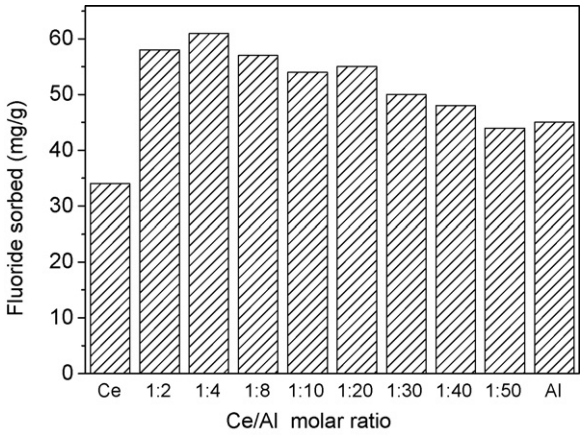

Fig. 2. Sorption of fluoride on the hybrid adsorbents prepared at different Ce/Al molar ratio (sorption conditions: 0.01 g adsorbent in 100 mL of 10 mg L^{-1} fluoride solution at pH 6 and 25 °C for 24 h).

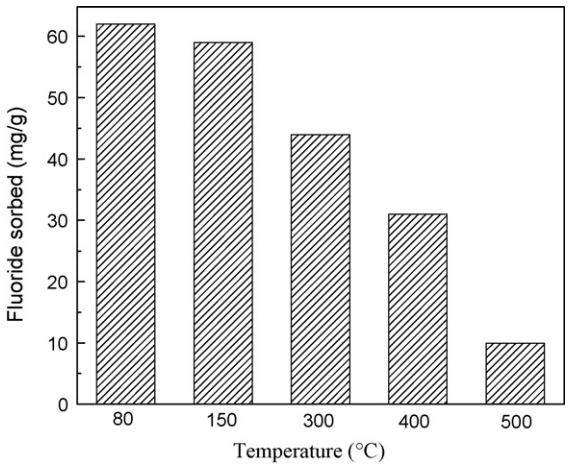

Fig. 3. Effect of drying temperature on the sorption of fluoride on the Al–Ce adsorbent (sorption conditions: 0.01 g adsorbent in 100 mL of 10 mg L^{-1} fluoride solution at pH 6 and 25 °C for 24 h)

is in agreement with the previous finding that La(III), Ce(IV), and Zr(IV) oxides had high sorption capacity for fluoride [13,14]. Among the four hybrid adsorbents, the Al–Ce adsorbent had the highest sorption capacity up to 62 mg g^{-1}, and thus its preparation conditions were optimized. The specific surface areas for the Al–Ti, Al–Ce, Al–La, Al–Zr and alumina adsorbents were 136.9, 60.1, 62.7, 121.7, 2.3 m^2 g^{-1}, respectively, indicating that their specific surface area was not a key factor for the sorption capacity. Instead, the special characteristic of rare earth elements may be responsible for the high sorption capacity of fluoride on the Al–Ce and Al–La adsorbents.

3.1.2. Effect of cerium content

Fig. 2 shows the effect of Ce/Al molar ratio on the sorption of fluoride on the adsorbent. The concentration of $AlCl_3$ was kept constant to be 0.2 mol L^{-1}, while the concentration of $Ce(NO_3)_3$ was variable from 0.1 mol L^{-1} to 4 mmol L^{-1}. It can be seen that the adsorption capacity increased first and then decreased with increasing Ce/Al ratio from 1:2 to 1:50, and the maximum sorption capacity was achieved at the Ce/Al ratio of 1:4. At the same time, the control adsorbents prepared with only $AlCl_3$ or $Ce(NO_3)_3$ were also used to adsorb fluoride under the same conditions. It is noticeable that the amount of fluoride adsorbed on the aluminum adsorbent was 45 mg g^{-1}, comparable to that on the composite adsorbent prepared at the Ce/Al molar ratio of 1:50, while the adsorption capacity of the cerium adsorbent for fluoride was 34 mg g^{-1}, far below the maximum sorption capacity on the adsorbent prepared at the Ce/Al molar ratio of 1:4.

The adsorbents made from aluminum and cerium compounds had the specific surface area of 2.3 and 136.8 m^2 g^{-1}, respectively. The Al–Ce adsorbents prepared at Ce/Al molar ratio of 1:4, 1:8, 1:20 had the specific surface area of 60.1, 64.9, 75.7 m^2 g^{-1}, respectively. It can be seen that the specific surface area is not a major factor affecting sorption capacity. Although the cerium oxide adsorbent had the highest surface area, its sorption capacity was the lowest. The above result indicated the synergistic interaction between aluminum and cerium compounds in the hybrid adsorbents, and the specific structure favorable for fluoride adsorption formed in the hybrid adsorbent.

3.1.3. Effect of drying temperature

Drying temperature in the adsorbent preparation had significant effect on the sorption of fluoride. After the precipitate was produced at the Ce/Al molar ratio of 1:4 and filtered, the obtained cake was dried in an oven at 80–500 °C for 10 h. As shown in Fig. 3, the sorption capacity decreased with increasing drying temperature, and the adsorbent dried at 80 °C and 150 °C had high sorption capacity for fluoride, while the sorption capacity was only 10 mg g^{-1} when the adsorbent was dried at 500 °C. In the preparation process, the obtained precipitate was aluminum and cerium hydroxides, and they were changed to oxides at high drying temperature. It was reported that the hydroxyl groups on the metal oxides were responsible for fluoride adsorption [20], and the decrease or loss of hydroxyl groups would decrease the sorption capacity on the adsorbents. It should be pointed out that the surface area of Al–Ce hybrid adsorbent decreased from 60.1 to 48.2 m^2 g^{-1} when the drying temperature increased from 80 °C to 400 °C, which may also cause the decrease of sorption capacity.

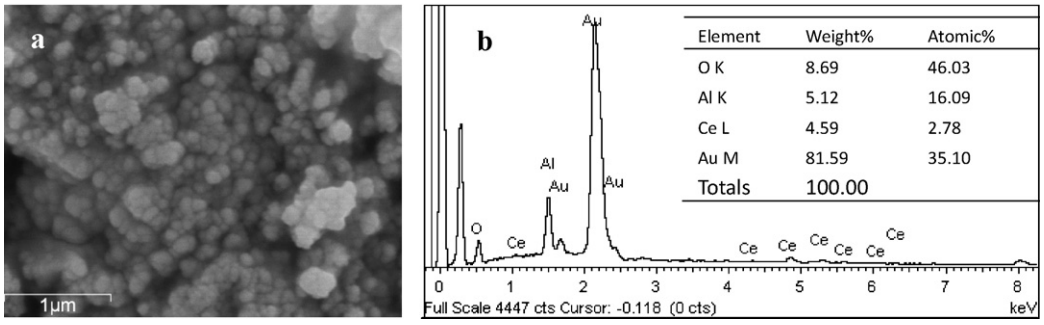

Fig. 4. SEM micrograph (a) and EDX surface analysis (b) of the Al–Ce adsorbent.

3.2. Adsorbent characterization

3.2.1. Surface morphology

The surface morphology and element composition on the surface of Al–Ce adsorbent prepared at the Ce/Al molar ratio of 1:4 and drying temperature of 80 °C were investigated by SEM-EDX. As illustrated in Fig. 4, the micrograph showed that the adsorbent was constituted by some aggregated nanoparticles at different sizes, which led to the rough surface and porous structure. It is estimated that the nanoparticles on the adsorbent surface were in the size range of 100–300 nm. The EDX analysis revealed that the elements of Al, Ce, Au and O were present on the adsorbent surface, and the Al/Ce molar ratio on the surface was about 5.8, a little higher than that in the preparation.

3.2.2. XRD analysis

The X-ray diffraction (XRD) pattern of the Al–Ce adsorbent prepared at different Al/Ce molar ratio and drying temperature as well as the alumina and cerium adsorbents are shown in Fig. 5. The moderate crystalline peaks can be seen in Fig. 5a, which can be attributed to boehmite (AlOOH). During the drying process, the produced $Al(OH)_3$ precipitate was converted to crystalline AlOOH at 80 °C in this study, and it would further changed to alumina (Al_2O_3) after being calcinated at 550 °C, which had different crystalline peaks from that of boehmite [21]. As shown in Fig. 5b, the cerium adsorbent prepared exhibited the distinct peaks at 28.7°, 33.1°, 47.6°, and 56.4°, indicating the presence of crystalline CeO_2 [22]. It is interesting to find that no crystalline peaks appeared in Fig. 5c and d for the Al–Ce adsorbent prepared through the coprecipitation of Al and Ce compounds at different ratios, suggesting the amorphous phase in the hybrid adsorbent at the drying temperature of 80 °C. As shown in Fig. 5e, the amorphous structure of adsorbent was destroyed at a drying temperature of 400 °C. CeO_2 (marked black) and Al_2O_3 (marked green) were found to present in the adsorbent. The sorption capacity decreased when the drying temperature increased from 80 °C to 400 °C. Obviously, the sorption capacity is related to the amorphous structure of the adsorbents, while the specific surface area is not a dominant factor for the sorption capacity according to our previous results.

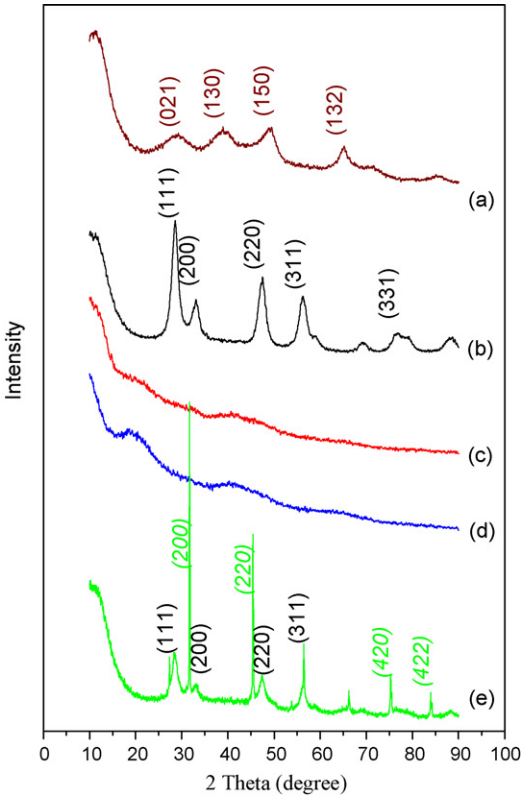

Fig. 5. XRD patterns of the adsorbents made from (a) aluminum chloride, (b) cerium nitrate, (c) aluminum chloride and cerium nitrate at Al/Ce molar ratio of 4:1, drying temperature at 80 °C, (d) Al/Ce molar ratio of 20:1, drying temperature at 80 °C, and (e) Al/Ce molar ratio of 4:1, drying temperature at 400 °C.

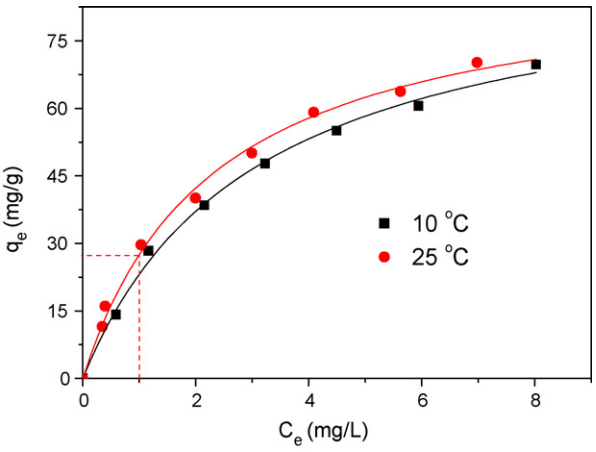

Fig. 6. Sorption isotherms of fluoride on the Al–Ce adsorbent at 25 °C and 10 °C.

Wu et al. also reported that the destruction of the amorphous structure of the trimetallic adsorbent at high calcination temperature caused the decrease of sorption capacity for fluoride [20]. This result also indicates that the hybrid adsorbent was not the simple mixture of AlOOH and CeO_2, and Al and Ce might form the complex compounds in the adsorbent. Since the hybrid adsorbent was not calcined, the metal phase should be hydroxide, which was confirmed by the following FTIR analysis.

3.3. Sorption isotherm

The best Al–Ce adsorbent prepared at Ce/Al molar ratio of 1:4 at drying temperature of 80 °C was used to investigate the sorption behavior of fluoride. The sorption isotherms of fluoride on the Al–Ce adsorbent at 25 °C and 10 °C are shown in Fig. 6. It can be found that the sorption capacity at equilibrium (q_e) gradually increased with increasing equilibrium fluoride concentrations, and the fluoride amount adsorbed at 25 °C was a little higher than that at 10 °C.

Langmuir equation has been successfully applied to model many sorption processes to evaluate the maximum sorption capacity of an adsorbate on an adsorbent [23,24]. Fig. 6 shows the modeling result using the Langmuir equation and the corresponding parameters for the plot are given in Table 1. It can be seen that the Langmuir model fitted the experimental data well according to the high correlation coefficients (R^2). The thermodynamic parameters for fluoride sorption on the Al–Ce adsorbent were also calculated. The negative values of ΔG° indicate that the sorption of fluoride on the adsorbent was spontaneous under the experimental conditions. ΔS° and ΔH° are calculated to be 0.113 kJ (mol K)$^{-1}$ and 11.473 kJ mol^{-1}, respectively. The positive value of the enthalpy change (ΔH°) indicates that the fluoride sorption process on the adsorbent is definitely endothermic in nature, while the positive value of the entropy change (ΔS°) suggests that the fluoride adsorption on the adsorbent surface occurred with increasing entropy possible due to the release of lot of molecular water at the solid/liquid interface during the sorption process [19].

The maximum sorption capacity (q_m) of the Al–Ce adsorbent for fluoride reached 91.4 mg g^{-1} at 25 °C according to the Langmuir fitting. It was reported that the adsorption capacities on some

Table 1
Calculated equilibrium constants and thermodynamic parameters for fluoride sorption on the Al–Ce adsorbent.

T (°C)	Langmuir constants[A]			Thermodynamic parameters[B]		
	b (L mg^{-1})	q_m (mg g^{-1})	R^2	ΔG° (kJ mol^{-1})	ΔH° (kJ mol^{-1})	ΔS° (kJ (mol K)$^{-1}$)
10	0.328	93.7	0.994	−20.6	11.473	0.113
25	0.431	91.4	0.994	−22.3		

[A] $q_e = q_m C_e/(1/b + C_e)$ [25].
[B] $\Delta G^\circ = -RT\ln b$ $\Delta G^\circ = \Delta H^\circ - T\Delta S^\circ$ [26].

Table 2
Comparison of adsorption capacity of some adsorbents for fluoride.

Adsorbents	pH	Equilibrium concentration (mg L^{-1})	Sorption capacity[a] (mg g^{-1})	References
Activated carbon	7.0	1	0.075	[9]
Bone char	7.0	1	2.71	[9]
Polymeric resin	7.0	1	3.62	[9]
Activated alumina	7.0	1	0.96	[9]
Ferric hydroxide	6.0–7.0	1	~3	[6]
$Fe_2O_3{\cdot}Al_2O_3{\cdot}xH_2O$	4.0	1	~30	[27]
Iron–aluminum mixed oxide	6.9	1.5	12	[19]
$MgAl{-}CO_3$ double hydroxides[b]	6.0	2	10	[11]
Fe–Al–Ce trimetal oxide[b]	7.0	1	12.2	[20]
Zr-impregnated collagen fiber	5.0–8.0	1	14.5	[17]
Activated kaolinite[b]	6.0	1	0.08	[12]
Laterite[b]	7.5	2.5	0.3	[28]
Titanium rich bauxites[b]	6.0	1	1.2	[29]
Macrophyte biomass	6.0	0.8	0.2	[30]
Al–Ce hybrid adsorbent[b]	6.0	1	27.5	This study

[a] Calculated from the sorption isotherms or Langmuir equation.
[b] Powder adsorbent.

adsorbents were high at high equilibrium concentration of fluoride [11], but in actual water treatment, the final concentration of fluoride must be below 1 mg L^{-1}. Therefore, the sorption capacity at low fluoride concentration is extremely important. As plotted in Fig. 6, the sorption capacity of the Al–Ce adsorbent for fluoride was about 27.5 mg g^{-1} at the equilibrium concentration of 1 mg L^{-1} at 25 °C.

For different adsorbents, the adsorption capacity for fluoride can be compared by calculating the amount of fluoride adsorbed on the adsorbents at the equilibrium fluoride concentration of 1 mg L^{-1}. Table 2 lists the sorption capacity of some adsorbents reported in the literature, and it can be found that the sorption capacities of the commercial available adsorbents such as activated alumina, bone char, and polymeric resin are 0.96, 2.71, and 3.62 mg g^{-1}, respectively. In recent years, some composite (hydr)oxides with high sorption capacity for fluoride have been developed. Wu et al. reported that the sorption capacity of the trimetallic oxides reached 12.2 mg g^{-1} at the equilibrium fluoride concentration of 1 mg L^{-1}. In Table 2, it can be seen that the Zr-impregnated collagen fiber had a high sorption capacity up to 14.5 mg g^{-1} for fluoride, and some researchers also reported that the hybrid adsorbents containing La(III), Ce(IV), and Zr(IV) had high sorption capacity for fluoride [15,17], but the addition of these metals in the preparation increased the cost of the adsorbents. As shown in Table 2, some cost-effective natural adsorbents including activated kaolinite, laterite, titanium rich bauxites, and macrophyte biomass were used to remove fluoride, but their sorption capacities are not satisfactory. The sorption capacity of the Al–Ce hybrid adsorbent prepared in this study was up to 27.5 mg g^{-1}, higher than that of almost all adsorbents except the $Fe_2O_3{\cdot}Al_2O_3{\cdot}xH_2O$ adsorbent. However, the sorption capacity of the $Fe_2O_3{\cdot}Al_2O_3{\cdot}xH_2O$ for fluoride was obtained at pH 4, and actually its sorption capacity at pH 6 was less than that of the Al–Ce adsorbent. It is notable that the Al–Ce adsorbent used in this study is in the form of powder, and the sorption capacity of the granular one for fluoride should be lower than this value.

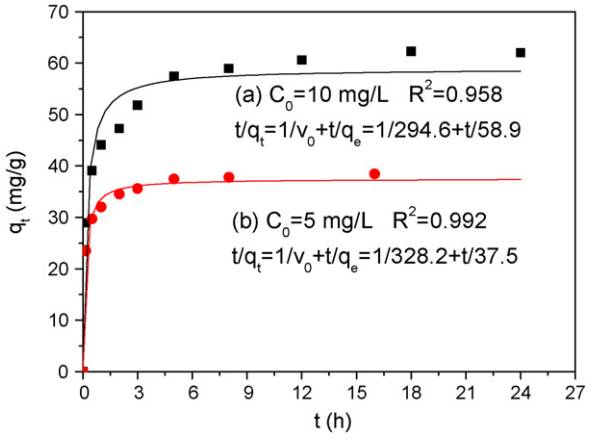

Fig. 7. Sorption kinetics of fluoride on the Al–Ce adsorbent at different initial fluoride concentration. Symbol: experimental data; curve: modeling results using the pseudo-second-order equation.

3.4. Sorption kinetics

The sorption kinetics of fluoride at different initial concentrations on the Al–Ce adsorbent is shown in Fig. 7. The sorption equilibrium was achieved within 5 h when the initial fluoride concentration was 5 mg L^{-1}, while it required 12 h to reach the equilibrium for the initial fluoride concentration of 10 mg L^{-1}.

The pseudo-second-order equation ($t/q_t = 1/\upsilon_0 + t/q_e$, υ_0 represents the initial sorption rate) is often adopted to evaluate the sorption rate of adsorbate on an adsorbent, which was used to describe chemisorption and has been widely applied to the adsorption of pollutants from aqueous solution in recent years [23,31]. As shown in Fig. 7, the pseudo-second-order kinetic model described the data obtained at initial concentration of 5 mg L^{-1} better than that at 10 mg L^{-1}. When the initial fluoride concentration was 5 mg L^{-1}, the initial sorption rate (υ_0) was 328.2 mg (g h)$^{-1}$.

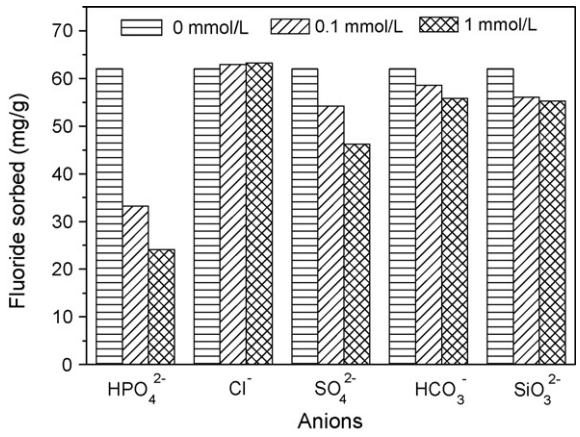

Fig. 8. Effect of co-existing anions on the sorption of fluoride on the Al–Ce adsorbent.

3.5. Effect of co-existing anions

In consideration of some anions commonly existed in actual groundwater, the effects of phosphate, sulfate, silicate, carbonate, and chloride on the sorption of fluoride on the adsorbent were studied. As presented in Fig. 8, these anions at different concentrations (0.1 and 1 mmol L^{-1}) had different effects on the sorption. Hydrogen phosphate caused the greatest decrease in fluoride sorption among the anions, while chloride had no effect on the sorption. Their effects on fluoride sorption followed the decreasing order of $HPO_4^{2-} > SO_4^{2-} > SiO_3^{2-} > HCO_3^- > Cl^-$. Many studies also showed that phosphate ions significantly interfered with fluoride sorption on chitosan beads and granular ferric hydroxide [6,32]. Fortunately, phosphate concentration in groundwater is normally low, and its effect on the fluoride sorption is limited.

3.6. Effect of solution pH

The sorption experiments were conducted in the pH range of 4.5–9.7 to investigate the effect of solution pH on the sorption fluoride on the Al–Ce adsorbent. As shown in Fig. 9, the sorption capacity changed little at pH below 6 and then decreased gradually with increasing solution pH when the solution pH was controlled during the sorption process. Obviously, this adsorbent had good sorption behavior in acidic solution, but the sorption capacity can still reached 53.2 mg g^{-1} at pH 7.8, little less than the highest value obtained at pH 6. In the experiment, it was found that the solution pH increased during the sorption process in acidic solution and the addition of HCl solution was required to maintain the constant solution pH, indicating the exchange of hydroxyl groups on

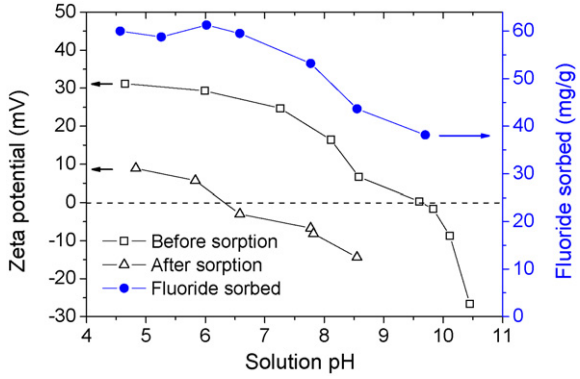

Fig. 9. Effect of solution pH on the fluoride sorption and zeta potentials on the Al–Ce adsorbent before and after fluoride sorption.

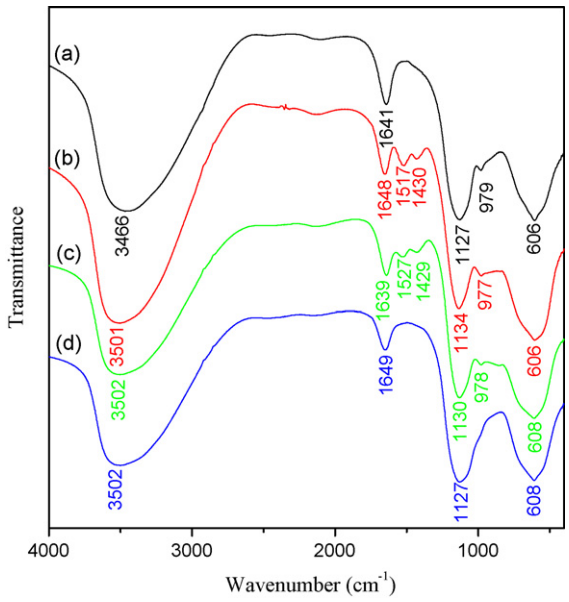

Fig. 10. FTIR spectra of (a) the Al–Ce adsorbent, (b) Al–Ce adsorbent after fluoride sorption, (c) Al–Ce adsorbent after fluoride sorption in the presence of SO_4^{2-}, and (d) Al–Ce adsorbent after fluoride sorption in the presence of HPO_4^{2-}.

the adsorbent surface with fluoride or the protonation of hydroxyl groups on the adsorbent.

The higher sorption capacity at low solution pH was related to the surface charge of the Al–Ce adsorbent. Fig. 9 also presents the ζ potentials of the adsorbent before and after fluoride sorption. It can be seen that the zero point of ζ potential of the Al–Ce adsorbent prepared at the Ce/Al ratio of 1:4 was at pH 9.6, indicating the positive surface charge of the adsorbent at pH < 9.6. The higher zero point of ζ potential of the Al–Ce adsorbent may be related to the composition of aluminum in the hybrid adsorbent [8]. Therefore, the positive adsorbent can be expected to provide better sorption for negative fluoride via electrostatic attraction. It also can be found that the zero point of ζ potential of the adsorbent after fluoride sorption decreased to 6.3, suggesting that the negative fluoride adsorbed on the positive sites and neutralized some positive charges on the adsorbent surface.

3.7. FTIR analysis

Fig. 10 shows the FTIR spectra of the Al–Ce adsorbent before and after fluoride adsorption. The broad band at 3466 cm^{-1} in the spectrum of the Al–Ce adsorbent can be assigned to the stretching vibration of adsorbed water, and the peak at 1641 cm^{-1} is attributed to the bending vibration of OH group [19]. The peaks observed between 1200 and 400 cm^{-1} were the characteristic vibrations of mixed metals. The strong peak at 1127 cm^{-1} can be assigned to the bending vibration of hydroxyl groups on metal oxides (M–OH) [33]. The strong band at 606 cm^{-1} is the characteristic of metal–oxygen vibration, which is attributed to Al–O bond in the adsorbent [34]. After fluoride adsorption, the bands at 3466 and 1641 cm^{-1} were shifted to 3501 and 1648 cm^{-1}, respectively, which corroborated the interaction of fluoride with the hydroxyl groups on the sorbent. It is interesting that the new peaks at 1517 and 1430 cm^{-1} appeared in the spectrum of the fluoride-sorbed adsorbent, which may be due to the Ce–F and Al–F bonds formed after fluoride adsorption [35]. The adsorbents after fluoride sorption in the presence of 1 mM SO_4^{2-} or HPO_4^{2-} obtained in Fig. 8 were analyzed by FTIR. As shown in Fig. 10c and d, the peaks at 1517 and 1429 cm^{-1} were weakened after fluoride sorption in the presence of SO_4^{2-}, while the two peaks almost disappeared after fluoride sorption in the pres-

ence of HPO_4^{2-}, which was associated with their significant effect on the sorption of fluoride on the Al–Ce adsorbent.

Based on the zeta potential measurement and FTIR analysis, the possible sorption mechanisms of fluoride on the Al–Ce adsorbent were proposed. At pH < 9.6, especially in acidic solution, the hydroxyl groups were protonated and the electrostatic interaction dominated the sorption. The high zero point of ζ potential and the increase of solution pH after fluoride sorption in the acidic solution verified this mechanism.

$$\equiv MOH_{(s)} + H^+_{(aq)} \rightleftarrows \equiv MOH_2{}^+_{(s)} \quad (1)$$

$$\equiv MOH_2{}^+_{(s)} + F^-_{(aq)} \rightleftarrows \equiv MF_{(s)} + H_2O \quad (2)$$

where ≡M represents the adsorbent surface.

At high solution pH, fluoride ions were possibly adsorbed by the following ion-exchange mechanism. The excessive amount of hydroxyl ions can compete for the active sites in the sorption process, resulting in the low sorption capacity for fluoride. Many researchers also proposed the similar sorption mechanism of fluoride on the metal oxides [20].

$$\equiv MOH_{(s)} + F^-_{(aq)} \rightleftarrows \equiv MF_{(s)} + OH^- \quad (3)$$

4. Summary

The Al–Ce hybrid adsorbent with high sorption capacity for fluoride was successfully prepared through the coprecipitation method. The optimal adsorbent was obtained by neutralizing the mixture containing 0.2 mol L^{-1} $AlCl_3$ and 0.05 mol L^{-1} $Ce(NO_3)_3$, and then the precipitate was dried at 80 °C. The composite adsorbent was composed of amorphous aluminum and cerium (hydr)oxides, and the hydroxyl groups on the adsorbent surface played an important role in the sorption. As the zero point of ζ potential of the Al–Ce adsorbent was at about pH 9.6, the anionic fluoride can easily adsorb on the positive adsorbent via electrostatic interaction. The adsorption of fluoride on the adsorbent was fast, and the maximum adsorption capacity was achieved at about pH 6. Among the five competing anions studied, phosphate ions significantly interfered with fluoride sorption. The Langmuir equation described the sorption isotherms well with a maximum sorption capacity of 91.4 mg g^{-1} obtained. The adsorbent had high sorption capacity up to 27.5 mg g^{-1} for fluoride at equilibrium fluoride concentration of 1 mg L^{-1}, much higher than that of some conventional adsorbents. The Al–Ce hybrid adsorbent has a promising application in the defluoridation of drinking water.

Acknowledgments

This research was supported by Program for New Century Excellent Talents in University. The analytical work was supported by the Laboratory Found of Tsinghua University. Additionally, Mr. Li Kaichong from China University of Mining & Technology is gratefully acknowledged for his participation in part of this research.

References

[1] I. Abe, S. Iwasaki, T. Tokimoto, N. Kawasaki, T. Nakamura, S. Tanada, Adsorption of fluoride ions onto carbonaceous materials, J. Colloid Interface Sci. 275 (2004) 35–39.
[2] WHO, Chemical fact sheets: fluoride, Guidelines for Drinking Water Quality: Incorporation First Addendum. Recommendations, vol. 1, third ed., Geneva, pp. 375–377, 2006.
[3] S.M. Maliyekkal, A.K. Sharma, L. Philip, Manganese-oxide-coated alumina: a promising sorbent for defluoridation of water, Water Res. 40 (2006) 3497–3506.
[4] W.M. Ding, T. Hairet, X. Huang, Primary study of fluoride removal from aqueous solution by activated ferric hydroxide, in: 2nd International Conference on Bioinformatics and Biomedical Engineering (ICBBE'08), 2008, pp. 2911–2913.
[5] M. Tahaikt, A.A. Haddou, R. El Habbani, Z. Amor, F. Elhannouni, M. Taky, M. Kharif, A. Boughriba, M. Hafsi, A. Elmidaoui, Comparison of the performances of three commercial membranes in fluoride removal by nanofiltration, Continuous Oper. Desalination 225 (2008) 209–219.
[6] E. Kumar, A. Bhatnagar, M. Ji, W. Jung, S.H. Lee, S.J. Kim, G. Lee, H. Song, J.Y. Choi, J.S. Yang, B.H. Jeon, Defluoridation from aqueous solutions by granular ferric hydroxide (GFH), Water Res. 43 (2009) 490–498.
[7] Z. Amor, B. Bariou, N. Mameri, M. Taky, S. Nicolas, A. Elmidaoui, Fluoride removal from brackish water by electrodialysis, Desalination 133 (2001) 215–223.
[8] A.L. Valdivieso, J.L.R. Bahena, S. Song, R.H. Urbina, Temperature effect on the zeta potential and fluoride adsorption at the α-Al_2O_3/aqueous solution interface, J. Colloid Interface Sci. 298 (2006) 1–5.
[9] N.A. Medellin-Castillo, R. Leyva-Ramos, R. Ocampo-Perez, R.F.G. de la Cruz, A. Aragon-Pina, J.M. Martinez-Rosales, R.M. Guerrero-Coronado, L. Fuentes-Rubio, Adsorption of fluoride from water solution on bone char, Ind. Eng. Chem. Res. 46 (2007) 9205–9212.
[10] N. Viswanathan, S. Meenakshi, Role of metal ion incorporation in ion exchange resin on the selectivity of fluoride, J. Hazard. Mater. 162 (2009) 920–930.
[11] L. Lv, J. He, M. Wei, D.G. Evans, Z.L. Zhou, Treatment of high fluoride concentration water by MgAl-CO_3 layered double hydroxides: kinetic and equilibrium studies, Water Res. 41 (2007) 1534–1542.
[12] S. Meenakshi, C.S. Sundaram, R. Sukumar, Enhanced fluoride sorption by mechanochemically activated kaolinites, J. Hazard. Mater. 153 (2008) 164–172.
[13] A.M. Raichur, M.J. Basu, Adsorption of fluoride onto mixed rare earth oxides, Sep. Purif. Technol. 24 (2001) 121–127.
[14] S. Tokunaga, M.J. Haron, S.A. Wasay, K.F. Wong, K. Laosangthum, A. Uchiumi, Removal of fluoride ions from aqueous solution by multivalent metal compounds, Int. J. Environ. Stud. 48 (1995) 17–23.
[15] K. Biswas, D. Bandhoyapadhyay, U.C. Ghosh, Adsorption kinetics of fluoride on iron(III)-zirconium(IV) hybrid oxide, Adsorption 13 (2007) 83–94.
[16] S.P. Kamble, S. Jagtap, N.K. Labhsetwar, D. Thakare, S. Godfrey, S. Devotta, S.S. Rayalu, Defluoridation of drinking water using chitin, chitosan and lanthanum-modified chitosan, Chem. Eng. J. 129 (2007) 173–180.
[17] X.P. Liao, B. Shi, Adsorption of fluoride on zirconium(IV)-impregnated collagen fiber, Environ. Sci. Technol. 39 (2005) 4628–4632.
[18] S. Samatya, U. Yuksel, M. Yuksel, N. Kabay, Removal of fluoride from water by metal ions (Al^{3+}, La^{3+} and ZrO^{2+}) loaded natural zeolite, Sep. Sci. Technol. 42 (2007) 2033–2047.
[19] K. Biswas, S.K. Saha, U.C. Ghosh, Adsorption of fluoride from aqueous solution by a synthetic iron(III)-aluminum(III) mixed oxide, Ind. Eng. Chem. Res. 46 (2007) 5346–5356.
[20] X.M. Wu, Y. Zhang, X.M. Dou, M. Yang, Fluoride removal performance of a novel Fe–Al–Ce trimetal oxide adsorbent, Chemosphere 69 (2007) 1758–1764.
[21] K.M. Parida, A.C. Pradhan, J. Das, N. Sahu, Synthesis and characterization of nano-sized porous gamma-alumina by control precipitation method, Mater. Chem. Phys. 113 (2009) 244–248.
[22] Z.H. Zhu, D.H. He, CO hydrogenation to iso-C4 hydrocarbons over CeO_2–TiO_2 catalysts, Fuel 87 (2008) 2229–2235.
[23] S.B. Deng, G. Yu, S.H. Xie, Q. Yu, J. Huang, Y. Kuwaki, M. Iseki, Enhanced adsorption of arsenate on the aminated fibers: sorption behavior and uptake mechanism, Langmuir 24 (2008) 10961–10967.
[24] S.B. Deng, Y.P. Ting, Polyethylenimine-modified fungal biomass as a high-capacity biosorbent for Cr(VI) anions: sorption capacity and uptake mechanisms, Environ. Sci. Technol. 39 (2005) 8490–8496.
[25] S.B. Deng, Y.P. Ting, Removal of As(V) and As(III) from water with a PEI-modified fungal biomass, Water Sci. Technol. 55 (2007) 177–185.
[26] S.B. Deng, Y.P. Ting, Fungal biomass with grafted poly(acrylic acid) for enhancement of Cu(II) and Cd(II) biosorption, Langmuir 21 (2005) 5940–5948.
[27] N.I. Chubar, V.F. Samanidou, V.S. Kouts, G.G. Gallios, V.A. Kanibolotsky, V.V. Strelko, I.Z. Zhuravlev, Adsorption of fluoride, chloride, bromide, and bromate ions on a novel ion exchanger, J. Colloid Interface Sci. 291 (2005) 67–74.
[28] M. Sarkar, A. Banerjee, P.P. Pramanick, Use of laterite for the removal of fluoride from contaminated drinking water, J. Colloid Interface Sci. 302 (2006) 432–441.
[29] N. Das, P. Pattanaik, R. Das, Defluoridation of drinking water using activated titanium rich bauxite, J. Colloid Interface Sci. 292 (2005) 1–10.
[30] P. Miretzky, C. Munoz, A. Carrillo-Chavez, Fluoride removal from aqueous solution by Ca-pretreated macrophyte biomass, Environ. Chem. 5 (2008) 68–72.
[31] Y.S. Ho, Second-order kinetic model for the sorption of cadmium onto tree fern: a comparison of linear and non-linear methods, Water Res. 40 (2006) 119–125.
[32] N. Viswanathan, C.S. Sundaram, S. Meenakshi, Sorption behaviour of fluoride on carboxylated cross-linked chitosan beads, Colloid Surf. B 68 (2009) 48–54.
[33] Y. Zhang, M. Yang, X.M. Dou, H. He, D.S. Wang, Arsenate adsorption on an Fe-Ce bimetal oxide adsorbent: role of surface properties, Environ. Sci. Technol. 39 (2005) 7246–7253.
[34] R.A. Nyquist, R.O. Kagel, Infrared Spectra of Inorganic Compounds (3800–45 cm^{-1}), Academic Press, New York, 1971, pp. 208–209.
[35] Z. Sarbak, The effect of fluoride concentration and catalyst preparation method on structural and thermal properties of CoMo/Al_2O_3 catalysts, Cryst. Res. Technol. 32 (1997) 1007–1013.